Title
Serial perturbation of MinK in IKs implies an alpha-helical transmembrane span traversing the channel corpus.

Journal
Biophysical journal, 93(7)

ISSN
0006-3495

Authors
Chen, Haijun
Goldstein, Steve AN

Publication Date
2007-10-01

DOI
10.1529/biophysj.107.109702

Serial Perturbation of MinK in I_{Ks} Implies an α-Helical Transmembrane Span Traversing the Channel Corpus

Haijun Chen and Steve A. N. Goldstein
The Department of Pediatrics and Institute for Molecular Pediatric Sciences, Pritzker School of Medicine, University of Chicago, Chicago, Illinois

ABSTRACT I_{Ks} channels contain four pore-forming KCNQ1 subunits and two accessory MinK subunits. MinK influences surface expression, voltage-dependence of gating, conduction, and pharmacology to yield the attributes characteristic of native channels in heart. The structure and location of the MinK transmembrane domain (TMD) remains a matter of scrutiny. As perturbation of gating analysis has correctly inferred the peripheral location and α-helical nature of TMDs in pore-forming subunits, the method is applied here to human MinK. Tryptophan and Asparagine substitution at 23 consecutive sites yields perturbation with α-helical periodicity (residues 44–56) followed by an alternating impact pattern (residues 56–63). Arginine substitution across the span suggests that as few as eight sites are occluded from aqueous solution (residues 50–57). We favor a TMD model that is α-helical with the external portion of the span at a lipid-protein boundary and the inner portion within the channel corpus in complex interactions.

INTRODUCTION

Voltage-gated potassium channels contain four pore-forming α-subunits and accessory β-subunits that dictate cell-specific operation. MinK-related peptides (MiRPs) are β-subunits with a single transmembrane span that control surface expression, voltage-dependence and kinetics of gating, unitary conductance, ion selectivity, and pharmacology (1–3). Many α-subunits employ one or more of the five *KCNE*-encoded MiRPs (4). In the heart and ear, MinK assembles with KCNQ1 (previously, KvLQT1) to form slowly-activating, I_{Ks} potassium channels (5,6). Inherited mutations in MinK or KCNQ1 that decrease potassium flux are associated with cardiac arrhythmia and deafness (7–9); pathogenic missense variants in MinK are found in the external, membrane-crossing, and internal portions of the subunit (10).

MinK has an external N-terminus and a stretch of 23 hydrophobic residues bounded by charged amino acids that is thought to be the transmembrane domain (TMD, human residues 44–66). While some posit the TMD is at the I_{Ks} channel periphery (11,12), others argue the span traverses the interior of the channel to influence both the conduction pore and gating apparatus (13–20). Studies demonstrating that each I_{Ks} channel has two MinK subunits suggest that the pore is bilaterally symmetric (15,21).

Perturbation analysis employs substitution effects on protein function to infer structure. The large, hydrophobic residue Tryptophan (Trp) can disrupt tightly-packed regions while it is well tolerated at lipid-exposed and membrane-water interfaces (22,23). Reciprocally, charged and polar residues such as Arginine (Arg) and Asparagine (Asn), respectively, disdain lipid, enjoying energetic respite in water (23–25). Because the side chain of Arg is flexible and nonpolar, it can snorkel through lipid to expose the charged terminal moiety in water (25). Arg is therefore intolerant of ad hoc packing in protein or lipid but is found at membrane-water interfaces.

Corresponding to natural sequence variability, perturbation of gating by Trp substitution (with retesting of equivocal sites with Asn) supports extensive α-helical structure and location at the lipid-facing channel periphery for *Shaker* α-subunit TMD segments S1, S2, and S3 (26,27). Concurrent studies with Kv2.1 employing substitution with Alanine come to similar conclusions (28). Validating the strategy, these inferences about secondary structure and location are well supported by subsequent direct structural determination of the related Kv1.2 channel (29).

Here, we employ perturbation analysis to make inferences about the secondary structure, location, and length of the MinK TMD in I_{Ks} channels formed with human MinK and KCNQ1. First, the 23 predicted TMD residues were studied after alteration to Trp; if perturbation was limited, the site was also studied with Asn. Proceeding across the span from the outside, substitutions yielded perturbations consistent with approximately three α-helical turns with exposure to lipid and channel protein. Thereafter, substitutions produced an alternating impact pattern consistent with a β-sheet, an α-helix with two faces exposed to nonpermissive environments, or another complex interaction. Perturbations on Arg substitution suggest a span as short as eight residues is protected from water. Despite enunciated concerns regarding the predictive value of perturbation analysis with a channel that does not achieve steady-state on activation and a span that does not appear to reside fully at a protein-lipid interface, the model is consistent with prior studies of MinK.

Submitted March 29, 2007, and accepted for publication May 22, 2007.

Address reprint requests to S. A. N. Goldstein, E-mail: sangoldstein@uchicago.edu.

H. Chen's current address is Department of Pharmacology, Yale University School of Medicine, 333 Cedar Street, SHMB 309, New Haven, CT 06520.

Editor: Jian Yang.

0006-3495/07/10/2332/09 $2.00

doi: 10.1529/biophysj.107.109702

EXPERIMENTAL PROCEDURES

Molecular biology

Human KCNQ1 and MinK genes were expressed in pRAT, a dual-purpose vector for transcript production or CMV-based expression (30). Mutations were created by pfu-based mutagenesis and confirmed by automated DNA sequencing in both directions of final constructs. cRNA was synthesized using an mMessage mMachine kit (Ambion, Austin, TX) from the T7 promoter in pRAT and quantified by spectroscopy and comparison to control samples separated by electrophoresis.

Electrophysiology and data analysis

Oocytes isolated from *Xenopus laevis* frogs were defolliculated by collagenase treatment and injected with 46 nl of sterile water containing 5 ng of the pore-forming KCNQ1 subunit cRNA and 1 ng MinK WT or mutant cRNA, unless otherwise noted, and studied 48–60 h thereafter. Whole-oocyte currents were measured by two-electrode voltage-clamp (Oocyte Clamp, Warner Instruments, Hamden, CT) with constant perfusion (~1 ml/min, solution exchange < 3 s). All recordings were at room temperature. Electrodes were filled with 3 M KCl and had resistance 0.1–1.2 MΩ. Data were sampled at 1 kHz and filtered at 0.25 kHz. Data recording and analysis were performed using Pulse + PulseFit (HEKA Electronik, Lambrecht, Germany), PClamp (Axon, Sunnyvale, CA), Excel (Microsoft, Redmond, WA) and IGOR software packages (WaveMetrics, Lake Oswego, OR). Raw currents are shown in figures; for data analysis, leak correction was performed off-line to assess only slowly-activating currents. Threshold voltage for channel activity (V_{open}) was chosen as a test voltage producing a time-dependent current of over 70 nA at the end of pulse.

Solutions

Standard bath solution was ND-96 (in mM): 96 NaCl, 2 KCl, 1 $MgCl_2$, 1.8 $CaCl_2$, and 5 HEPES adjusted to pH 7.5 with NaOH.

Protocols

For measurement of channel activation, cells were depolarized to test voltages from –80 mV to +80 mV with 10 mV steps from a holding potential of −90 mV every 15 s, a 5 s interpulse interval, and tail currents were recorded at −50 mV. Application of charybdotoxin (CTX) was as previously described (15).

RESULTS

Perturbation of Trp and Asn substitution suggests protein or lipid contact

The 23 residues in the putative TMD of human MinK (Fig. 1 *A*) were first replaced individually by Trp and I_{Ks} channels formed with human KCNQ1 studied in *Xenopus laevis* oocytes by two-electrode voltage-clamp. Isochronal gating parameters for the mutants were compared with wild-type channels. The effects of mutations were studied isochronally because I_{Ks} channels do not reach steady state (13,31). Isochronal gating parameters offer, at best, an approximation of gating free energy since only equilibrium measurements yield state-independent free energies. The effects of MinK mutations were therefore analyzed by gating measurements at equivalent times to determine zero-voltage isochronal free energy of opening ($\Delta\Psi_{iso}$). Measured parameters included isochronal activation time to half-maximal amplitude ($T_{1/2}$), tail current deactivation time constant (τ_d), and threshold voltage for channel activity (V_{open}). Conductance-voltage curves were fitted with a Boltzmann relation, $G/G_{max} = (1+\mathrm{Exp}[-zF(V-V_{1/2})/RT])^{-1}$, where F, R, and T have their usual meanings, to obtain half-maximal activation voltage $V_{1/2}$, slope factor z, and evaluate the quasi-equilibrium $\Delta\Psi_{iso} = zFV_{1/2}$. Changes in isochronal free energy ($\Delta\Delta\Psi_{iso}$) were determined as the difference between $\Delta\Psi_{iso}$ for wild-type and mutant channels.

In all cases, Trp-substituted MinK subunits formed slowly-activating, I_{Ks}-like channels, although current density was too low with MinK-F57W to analyze in detail. Exemplar current traces for channels with wild-type MinK and three MinK mutants are presented in Fig. 1. Whereas MinK-G60W operated like wild-type (Fig. 1 *B*), MinK-A44W showed a hyperpolarizing shift in $V_{1/2}$ of ~−29 mV while MinK-G55W induced a depolarizing shift of ~+20 mV (Fig. 1 *C* and *D*). Thus, channels with MinK-A44W favor the open state compared to wild-type while those with MinK-G55W

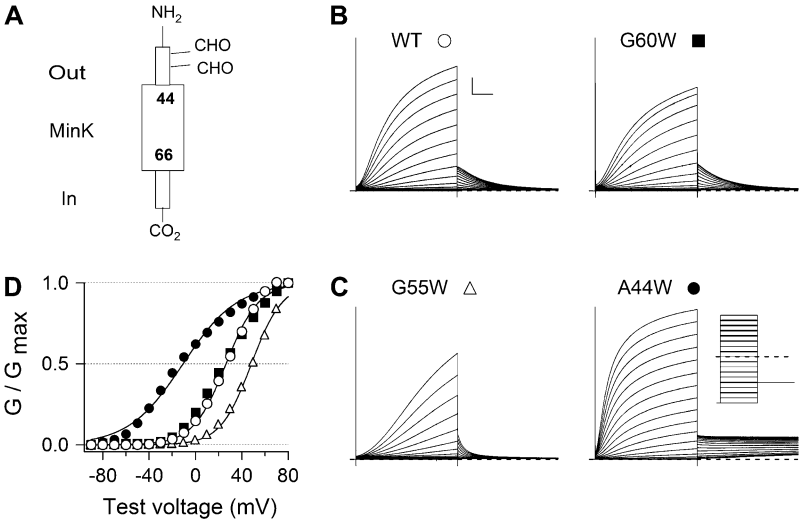

FIGURE 1 Activation of I_{Ks} channels with WT or Trp-substituted MinK mutants. (*A*) Topology of MinK, a Type I protein. (*B*) Whole-oocyte currents were recorded with two-electrode voltage clamp from I_{Ks} channels with wild-type MinK (*WT*) or MinK-G60W; (*C*) MinK-A44W or MinK-G55W. (*Inset*) Protocol, a family of 5-s test pulses from −90 to +80 mV with 10 mV increment from a hold potential of −90 mV. Tail currents were collected at −50 mV. Scale bar: 1 s and 1 μA. (*D*) MinK A44W and G55W significantly change the voltage dependence of activation in I_{Ks} channels. *G-V* curves obtained from recordings in panel *B*, panel *C* according to $G = I_{5s\ isochronal}/(V\text{-}E_K)$. Continuous lines are fits to a Boltzmann function to assess half-maximum activation voltage and slope factor. Data collected from several batches of oocytes (n = 15–35 oocytes).

prefer the closed state. Gating parameters for Trp-substituted channels are listed in Table 1.

Isochronal free energy differences between wild-type and Trp-substituted I_{Ks} channels ($\Delta\Delta\Psi_{iso}$) are presented in Fig. 2 *A* and Table 1. The intention of this analysis is to identify sites where mutations produce clear changes in isochronal gating parameters and not to explore mechanistic details in the activation pathway. Therefore, a demanding cutoff for high impact of substitutions was chosen. Setting the cutoff at $|\Delta\Delta\Psi_{iso}| > 0.9$ kcal/mol identified seven of the 23 MinK Trp mutants as those that yield I_{Ks} channels with gating energies markedly different from wild-type (A44, G55, F57, L59, I61, L63, S64, Table 1). Most high-impact sites also showed changes in gating kinetics that were greater than twofold (Tables 1 and 2) as found in studies of *Shaker* channel TMDs (27).

Sixteen I_{Ks} channels with Trp-substituted MinK subunits had properties similar to wild-type with $|\Delta\Delta\Psi_{iso}| < 0.9$ kcal/mol. Fourteen of these sites were studied by substitution with Asn to investigate if the small, polar residue might impact where the large, hydrophobic residue did not (Fig. 2 *A*, Table 2); G52 and G60 were judged to be adequately assessed by Trp substitution and not studied further (Table 1). Substitutions at three of the 14 sites had marked effects on gating (L45, Y47, and L51, Table 2). Overall, 10 of the 23 MinK residues tested were significantly impacted by Trp or Asn substitution (Fig. 2, sites boxed in *red*).

Inferred secondary structure

To seek evidence for α-helical periodicity in the impact of MinK mutants, the 23 residues were placed on a helical wheel model highlighting sites with $|\Delta\Delta\Psi_{iso}| > 0.9$ kcal/mol in red; an α-helical pattern was not apparent by inspection across the full span (Fig. 2 *B*), although residues 44–56 evaluated in isolation suggest three turns of this arrangement (Fig. 2 *C*). This impression is supported by Fourier periodicity analysis according to Li-Smerin and colleagues (28) that yielded a peak angle of 104° (within the expected range of 90–120°) with an α-periodicity index of 2.20 (>2 indicating high likelihood of an α-helix) for residues 44–56. Residues 56–63 showed an alternating pattern of impact consistent with an extended arrangement or an α-helix with two high-impact faces (Fig. 2 *D*).

Tolerance of Arg substitutions suggests aqueous contact

Tolerance of a nonconservative Arg substitution suggests access to the aqueous phase because the energy cost of burying the terminal moiety within the hydrophobic interior of the membrane lipid or the protein is unfavorable (23–25). Tolerance for Arg substitution was employed here to infer sites accessible to water and, by coincidence with tolerance

TABLE 1 Biophysical properties of I_{Ks} channels formed with Trp-substituted MinK mutants

MinK Site	$V_{1/2}$ (mV)	Z	$\Delta\Psi_{iso}$ (kcal/mol)	$\Delta\Delta\Psi_{iso}$ (kcal/mol)	τ_d (s)	$T_{1/2}$ (s)	V_{open} (mV)
WT	25.2 ± 1.3	1.50 ± 0.03	0.88 ± 0.05		1.23 ± 0.04	1.46 ± 0.05	−22.3 ± 1.2
A44W	−4.0 ± 1.3	1.24 ± 0.03	−0.12 ± 0.08	**−1.00**	>4	0.96 ± 0.03	−50.6 ± 1.4
L45W	37.5 ± 1.2	1.74 ± 0.05	1.52 ± 0.09	0.64	0.61 ± 0.03	1.66 ± 0.14	−6.7 ± 2.3
Y46W	39.2 ± 1.8	1.36 ± 0.04	1.26 ± 0.09	0.34	0.49 ± 0.02	1.60 ± 0.07	−23.1 ± 2.5
V47W	34.1 ± 0.9	1.26 ± 0.02	0.99 ± 0.04	0.11	1.73 ± 0.05	2.25 ± 0.12	−20.6 ± 2.0
L48W	23.7 ± 0.5	1.42 ± 0.01	0.77 ± 0.02	−0.11	1.80 ± 0.15	1.26 ± 0.05	−22.9 ± 1.8
M49W	29.5 ± 0.4	1.46 ± 0.02	0.99 ± 0.02	0.11	1.31 ± 0.08	1.60 ± 0.06	−22.5 ± 1.3
V50W	28.7 ± 0.8	1.47 ± 0.04	0.98 ± 0.04	0.10	0.90 ± 0.04	1.30 ± 0.05	−23.6 ± 1.3
L51W	28.8 ± 1.9	1.45 ± 0.04	0.97 ± 0.08	0.09	1.39 ± 0.10	1.89 ± 0.07	−25.7 ± 1.4
G52W	18.3 ± 1.4	1.42 ± 0.03	0.61 ± 0.08	−0.27	1.27 ± 0.08	1.43 ± 0.04	−25.7 ± 1.4
F53W	15.4 ± 1.6	1.48 ± 0.03	0.53 ± 0.06	−0.35	1.54 ± 0.10	1.29 ± 0.06	−27.1 ± 1.3
F54W	11.0 ± 1.9	1.35 ± 0.02	0.34 ± 0.09	−0.54	1.64 ± 0.17	1.05 ± 0.06	−33.4 ± 2.4
G55W	46.0 ± 1.6	1.86 ± 0.04	2.03 ± 0.04	**1.15**	0.59 ± 0.04	2.72 ± 0.09	0.7 ± 2.0
F56W	24.9 ± 0.8	1.48 ± 0.03	0.86 ± 0.04	−0.08	1.00 ± 0.02	1.41 ± 0.05	−23.2 ± 1.4
F57W	>100	ND	ND	**>1**	ND	ND	ND
T58W	25.1 ± 1.7	1.39 ± 0.01	0.81 ± 0.06	−0.07	0.34 ± 0.03	1.08 ± 0.09	−18.4 ± 2.3
L59W	−2.4 ± 2.0	1.47 ± 0.03	−0.09 ± 0.07	**−0.97**	0.81 ± 0.07	0.26 ± 0.03	−34.6 ± 2.0
G60W	22.7 ± 0.7	1.52 ± 0.03	0.80 ± 0.03	−0.08	0.99 ± 0.06	1.40 ± 0.06	−24.5 ± 1.8
I61W	42.0 ± 1.7	1.86 ± 0.03	1.81 ± 0.10	**0.93**	0.15 ± 0.01	1.17 ± 0.03	−1.3 ± 1.9
M62W	31.4 ± 0.5	1.55 ± 0.01	1.12 ± 0.02	0.24	0.76 ± 0.02	1.92 ± 0.03	−22.4 ± 1.4
L63W	44.3 ± 1.2	1.85 ± 0.05	1.92 ± 0.10	**1.04**	0.46 ± 0.01	1.95 ± 0.07	−0.00 ± 1.8
S64W	56.0 ± 0.6	2.43 ± 0.04	3.15 ± 0.08	**2.23**	0.16 ± 0.01	2.48 ± 0.03	15.6 ± 1.6
Y65W	13.8 ± 1.1	1.55 ± 0.11	0.50 ± 0.09	−0.38	1.32 ± 0.15	1.35 ± 0.06	−32.0 ± 2.5
I66W	28.4 ± 1.5	1.65 ± 0.03	1.08 ± 0.06	0.20	0.33 ± 0.02	0.84 ± 0.03	−20.6 ± 1.1

Data from 15–35 oocytes were fitted to a Boltzmann function as described in the Experimental Procedures. Seven high impact substitutions defined as those with $|\Delta\Delta\Psi_{iso}| > 0.9$ kcal/mol are noted in boldface. $V_{1/2}$, Z, $\Delta\Psi_{iso}$, $\Delta\Delta\Psi_{iso}$, τ_d, $T_{1/2}$, and V_{open} were determined as described in Results and Experimental Procedures. All values are mean ± SE. *ND* indicates not done. F57W was judged to have $V_{1/2} > 100$ mV but currents were too small (under 250 nA at +60 mV) to perform detailed analyses.

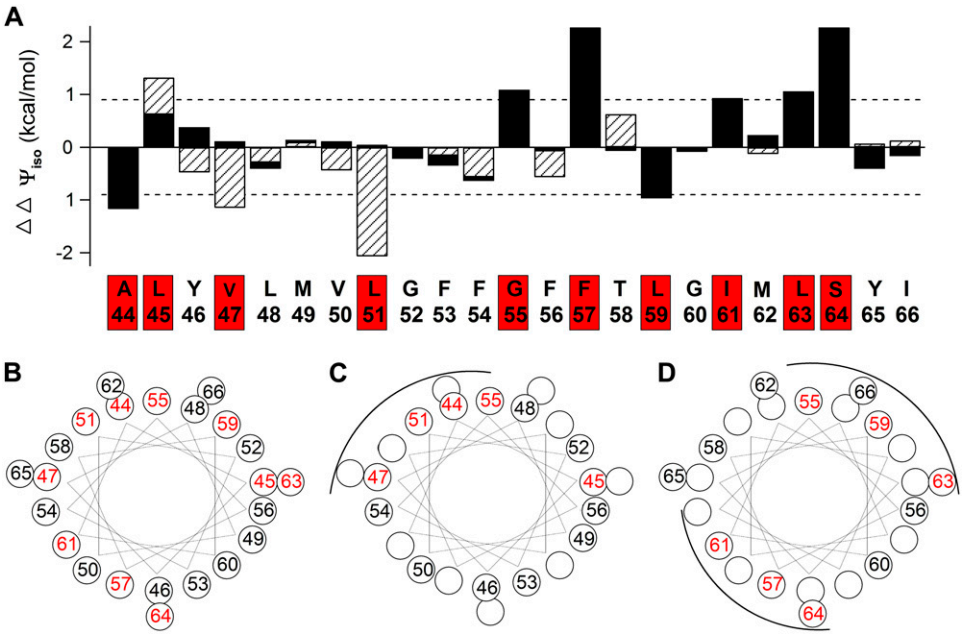

FIGURE 2 Some Trp or Asn-substituted MinKs perturb gating of I_{Ks} channels. (*A*) Change in isochronal free energy ($\Delta\Delta\Psi_{iso}$, see Experimental Procedures), induced by Trp (*solid bars*) or Asn (*hatched bars*) plotted versus the 23 residues studied in MinK. Dashed line indicates $|\Delta\Delta\Psi_{iso}| = 0.9$ kcal/mol. The 10 sites judged high-impact by Trp or Asn substitution are noted by a red box on the sequence. Data are collected from several batches of cells (n = 15–35 oocytes each condition). (*B*) Helical wheel residues studied (residues 44–66), high-impact site in red. (*C*) Helical wheel residues 44–56, high-impact sites are on one face in red. (*D*) Helical wheel residues 56–64, high-impact sites on two faces in red.

for Trp substitution, to infer the portion of the MinK TMD isolated from aqueous spaces. Arg substitution was not otherwise used to infer transmembrane secondary structure since it is expected to disrupt at sites exposed to both protein and lipid.

Eleven of the 23 residues substituted with Arg yielded biophysical behavior in I_{Ks} channels similar to those with wild-type MinK yielding $|\Delta\Delta\Psi_{iso}| < 0.9$ kcal/mol (Fig. 3, *A* and *D*, Table 3). Twelve of the sites were intolerant of substitution; eight had significant shifts in gating energies with $|\Delta\Delta\Psi_{iso}| > 0.9$ kcal/mol (Table 3) while four had slowly-activating, I_{Ks}-like currents that are too small to assess in detail (Fig. 3, *B* and *C*; G52, F53, F54, and L59). Disruption by Arg substitution at the 13 sites can be rationalized by effects of Trp and Asn substitution that support exposure of these sites to protein or lipid (Tables 1 and 2) and by studies suggesting their intimate association with the ion conduction pore (13,16,18) and portions of the channel that control gating (20).

Overlapping tolerance of Arg and Trp substitution is seen at seven sites (Fig. 3 *D*, sites boxed in *green*); these include residues L48/M49 and T58/G60, suggesting the minimal occluded portion between external and internal aqueous spaces is eight residues.

TABLE 2 Biophysical properties of I_{Ks} channels formed with Asn-substituted MinK mutants

MinK Site	$V_{1/2}$ (mV)	Z	$\Delta\Psi_{iso}$ (kcal/mol)	$\Delta\Delta\Psi_{iso}$	τ_d (s)	$T_{1/2}$ (s)	V_{open} (mV)
WT	25.2 ± 1.3	1.50 ± 0.03	0.88 ± 0.05		1.23 ± 0.04	1.46 ± 0.05	−22.3 ± 1.2
L45N	47.9 ± 1.1	1.98 ± 0.05	2.20 ± 0.09	**1.32**	0.41 ± 0.02	1.35 ± 0.08	−6.9 ± 2.1
Y46N	15.6 ± 0.7	1.11 ± 0.03	0.40 ± 0.06	−0.48	0.59 ± 0.07	0.49 ± 0.01	−42.0 ± 2.0
V47N	−9.3 ± 1.4	1.28 ± 0.04	−0.27 ± 0.04	**−1.15**	>5	0.93 ± 0.03	−47.4 ± 2.0
L48N	18.1 ± 1.1	1.43 ± 0.01	0.59 ± 0.04	−0.29	1.75 ± 0.04	1.40 ± 0.03	−27.3 ± 1.4
M49N	27.8 ± 1.0	1.44 ± 0.03	0.92 ± 0.04	0.04	1.64 ± 0.04	1.64 ± 0.07	−21.1 ± 2.0
V50N	14.0 ± 0.8	1.31 ± 0.02	0.42 ± 0.02	−0.46	1.84 ± 0.20	0.91 ± 0.04	−35.0 ± 1.7
L51N	−29.3 ± 1.4	1.77 ± 0.06	−1.19 ± 0.06	**−2.07**	0.88 ± 0.03	0.04 ± 0.01	−51.1 ± 1.1
F53N	20.4 ± 1.0	1.41 ± 0.03	0.67 ± 0.05	−0.21	0.73 ± 0.04	1.17 ± 0.05	−25.9 ± 1.1
F54N	9.0 ± 2.2	1.20 ± 0.02	0.24 ± 0.05	−0.64	2.18 ± 0.06	1.05 ± 0.06	−33.3 ± 2.4
F56N	9.0 ± 1.5	1.34 ± 0.02	0.27 ± 0.02	−0.61	1.28 ± 0.05	0.86 ± 0.04	−33.0 ± 1.5
T58N	36.6 ± 2.5	1.79 ± 0.05	1.51 ± 0.08	0.63	0.13 ± 0.01	1.91 ± 0.05	−10.2 ± 2.3
M62N	15.7 ± 1.5	1.32 ± 0.01	0.75 ± 0.01	−0.13	0.57 ± 0.03	0.75 ± 0.04	−25.4 ± 1.4
Y65N	27.1 ± 0.7	1.49 ± 0.02	0.93 ± 0.02	0.05	1.28 ± 0.05	0.90 ± 0.05	−22.5 ± 0.9
I66N	28.9 ± 1.2	1.42 ± 0.02	0.95 ± 0.05	0.07	1.18 ± 0.06	1.42 ± 0.08	−24.7 ± 1.3

Data from 15–35 oocytes were fitted to a Boltzmann function as described in the Results and Experimental Procedures. Three high-impact substitutions defined as those with $|\Delta\Delta\Psi_{iso}| > 0.9$ kcal/mol are noted in boldface. $V_{1/2}$, Z, $\Delta\Psi_{iso}$, $\Delta\Delta\Psi_{iso}$, τ_d, $T_{1/2}$, and V_{open} were determined as described in Experimental Procedures. All values are mean ± SE.

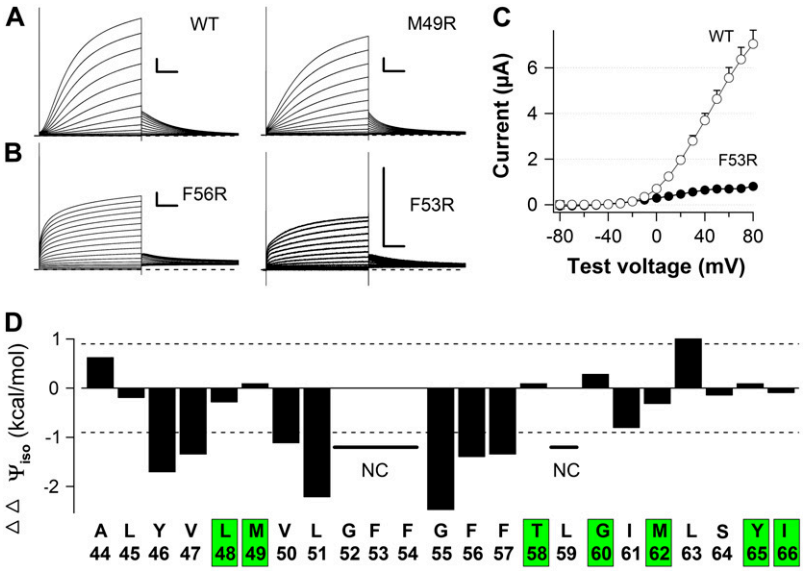

FIGURE 3 Some Arg-substituted MinKs do not alter gating of I_{Ks} channels. Arg-scanning was performed to determine the aqueous boundaries of the MinK transmembrane domain. Whole-oocyte currents were studies as in Fig. 1 *A* with several batches of oocytes ($n = 10$–20 oocytes each condition). Scale bar: 1 s and 1 μA. (*A*) Representative currents for I_{Ks} channels with wild-type MinK and a site that tolerated Arg substitution (50). (*B*) Representative currents for I_{Ks} channels with two sites that did not tolerate Arg substitution (residues 53 and 56). (*C*) *I/V* curves from recordings of cells as in *A* and *B*. (*D*) Of the 10 sites judged tolerant of Arg substitution (Table 3), seven sites are tolerant of Trp and Arg substitution and noted by a green box on the sequence. NC indicates not calculated.

Effects of Arg substitution on toxin binding in the pore

Charybdotoxin (CTX) inhibition of channels with Arg-substituted at MinK positions 48 or 49 was not different than with wild-type MinK when a toxin-sensitive variant of KCNQ1 is employed (MinK-L48R, MinK-M49R, and wild-type: $K_i = 12.8 \pm 2.6$, 14.1 ± 1.2, and 11.1 ± 2.3 nM; $K_{on} = 2.1 \pm 0.5$, 1.9 ± 0.3, and 1.8 ± 0.8 μM^{-1} s^{-1}; $K_{off} = 27.0 \pm 5.6 \times 10^{-3}$, $30.8 \pm 3.9 \times 10^{-3}$, and $23 \pm 5.1 \times 10^{-3}$ s^{-1}), by a method described previously (15). The lack of an effect of substitution at these sites on the affinity of the positively-charged toxin suggests the terminal Arg moiety is not in the outer vestibule or is shielded. Conversely, a charged epitope added in the external portion of MinK that precedes the TMD (between residues 30 and 31) increases the binding affinity of CTX by enhancing on-rate without significant changes in off-rate (15), consistent with a through-space electrostatic influence rather than changes in the toxin binding site (32).

DISCUSSION

Perturbation of gating by substitution with Trp and Asn was used to classify 23 residues in the TMD of MinK in I_{Ks} channels. Substitutions at 10 sites had major impact (Table 4, Fig. 4 *A*). Seven sites tolerate substitution with Trp and Arg, suggesting minimal boundaries for the portion of the TMD occluded from aqueous contact (Table 4, Fig. 4 *B*). Substitution effects suggest the TMD enters the membrane from the outside with ~3 α-helical turns (residues 44–56) and then manifests an alternating pattern (residues 56–63) consistent with an extended conformation, continuation in α-helical fashion with two interacting faces (the model we favor), or another complex set of interactions. The rationale for the proposed model, its relationship to prior studies, and limitations of the method that challenge the strength of the model follow.

The structural basis for MinK function has been a subject of controversy. MinK is demonstrated to be a Type I single-pass protein by glycosylation of residues N5 and N26, indicating the N-terminus is external (33) and phosphorylation of Ser^{103} showing the C-terminus is inside the cell (34). Side-specific antibody binding supports this topology (15). Based on studies of pore blockade and ion selectivity we have suggested that the MinK TMD travels from the lateral portion of the outer pore vestibule (13–15,17) toward the channel center, running close to the ion conduction pathway near the selectivity filter (13,16,18) and then passes near the inner pore vestibule without apparent contact with the aqueous solution (17).

Thus, open channel inhibition from the outside by small blockers, covalent modification of MinK sites, and binding of peptide toxins have identified portions of the external N-terminus (18,35) and TMD that are pore-associated (Table 4, Fig. 4 *C*) (13,14,17). Two adjacent residues (55 and 56) act as if pore-exposed on opposite sides of a filter that restricts transmembrane movement of sodium, cadmium, and zinc ions (Table 4, Fig. 4 *C*) (13,16,18). The TMD model we suggest here is consistent with these observations.

MinK TMD residues 44–55 show α-helical periodicity suggesting exposure at a protein-lipid interface. Lack of an effect on CTX blockade of Arg substitution at positions 48 and 49 argues that at least the charged terminal moiety is shielded or sufficiently distant from the pore to preclude steric and through-space electrostatic effects on binding of the positively-charged toxin. Despite an alternating impact pattern, residues 56–63 could continue in α-helical fashion if the segment enters the channel corpus to interact with protein on more than one face (Fig. 2 *D*).

TABLE 3 Biophysical properties of I_{Ks} channels formed with Arg-substituted MinK mutants

MinK Site	$V_{1/2}$ (mV)	Z	$\Delta\Psi_{iso}$ (kcal/mol)	$\Delta\Delta\Psi_{iso}$	τ_d (s)	$T_{1/2}$ (s)	V_o (mV)
WT	25.2 ± 1.3	1.50 ± 0.03	0.88 ± 0.05		1.23 ± 0.04	1.46 ± 0.05	−22.3 ± 1.2
A44R	39.6 ± 2.6	1.63 ± 0.07	1.51 ± 0.15	**0.63**	0.62 ± 0.04	1.94 ± 0.11	−10.0 ± 2.9
L45R	23.7 ± 1.6	1.23± 0.03	0.68 ± 0.06	**−0.20**	0.43 ± 0.01	0.85 ± 0.05	−28.3 ± 1.2
Y46R	−27.8 ± 4.0	1.29 ± 0.04	−0.83 ± 0.13	−1.71	1.04 ± 0.03	0.15 ± 0.02	−46.7 ± 6.7
V47R	−16.1 ± 3.2	1.27 ± 0.08	−0.47 ± 0.10	−1.35	0.93 ± 0.12	0.22 ± 0.06	−42.5 ± 2.5
L48R	21.1 ± 1.8	1.21 ± 0.02	0.59 ± 0.05	**−0.29**	1.38 ± 0.09	1.11 ± 0.04	−26.4 ± 1.5
M49R	28.5 ± 1.1	1.33 ± 0.02	0.88 ± 0.04	**0.00**	0.92 ± 0.02	1.31 ± 0.07	−23.8 ± 1.8
V50R	−7.8 ± 2.2	1.26 ± 0.05	−0.24 ± 0.10	−1.12	0.97 ± 0.07	0.43 ± 0.04	−43.8 ± 1.8
L51R	−31.0 ± 2.1	1.87 ± 0.05	−1.34 ± 0.11	−2.22	0.11 ± 0.03	1.14 ± 0.07	−55.3 ± 2.6
G55R	−37.8 ± 1.7	1.84 ± 0.05	−1.60 ± 0.09	−2.48	1.36 ± 0.14	0.04 ± 0.01	−60.8 ± 2.5
F56R	−18.9 ± 1.4	1.17 ± 0.03	−0.52 ± 0.04	−1.40	1.45 ± 0.13	0.28 ± 0.05	−45.8 ± 3.1
F57R	−21.7 ± 1.9	0.95 ± 0.05	−0.47 ± 0.03	−1.35	1.72 ± 0.12	0.21 ± 0.04	−51.8 ± 3.4
T58R	28.2 ± 2.4	1.38 ± 0.11	0.92 ± 0.14	**0.04**	0.24 ± 0.02	0.74 ± 0.11	−23.3 ± 4.2
G60R	32.8 ± 1.5	1.54 ± 0.03	1.17 ± 0.07	**0.29**	0.26 ± 0.01	0.97 ± 0.07	−17.5 ± 2.5
I61R	3.2 ± 5.3	1.02 ± 0.02	0.07 ± 0.12	**−0.81**	0.23 ± 0.03	0.08 ± 0.01	−50.3 ± 2.6
M62R	20.1 ± 1.9	1.26 ± 0.01	0.56 ± 0.06	**−0.32**	0.42 ± 0.02	0.85 ± 0.05	−26.7 ± 1.7
L63R	44.9 ± 0.8	1.83 ± 0.06	1.89 ± 0.09	1.01	0.18 ± 0.01	0.81 ± 0.08	−8.8 ± 3.5
S64R	23.4 ± 1.4	1.42 ± 0.03	0.73 ± 0.07	**−0.15**	0.54 ± 0.03	0.74 ± 0.05	−27.0 ± 2.1
Y65R	26.3 ± 0.9	1.58 ± 0.05	0.95 ± 0.02	**0.07**	0.50 ± 0.01	0.75 ± 0.05	−21.7 ± 1.7
I66R	25.0 ± 1.1	1.47 ± 0.02	0.84 ± 0.03	**−0.04**	0.48 ± 0.03	0.84 ± 0.05	−24.7 ± 1.3

Data from 15–25 oocytes were fitted to a Boltzmann function as described in the Experimental Procedures. Eleven low-impact substitutions defined as those with $|\Delta\Delta\Psi_{iso}| < 0.9$ kcal/mol are noted in boldface. $V_{1/2}$, Z, $\Delta\Psi_{iso}$, $\Delta\Delta\Psi_{iso}$, τ_d, $T_{1/2}$, and V_o were determined as described in Experimental Procedures. Four sites yielded Arg-substituted channels with slowly-activating, I_{Ks}-like currents that were too small to assess in biophysical detail (52, 53, 54, and 59, under 500 nA at +60 mV). All values are mean ± SE.

An α-helical structure of 20 residues (44–63) can span the membrane even if angled off normal. The average number of residues separating two sides of the membrane in 160 transmembrane helices in 15 nonhomologous high-resolution protein structures was 17.3 (with a distance of 26 Å) (36). The proposed structure is also consistent with the apparently short stretch of the span that is protected from water (residues 50–57) because Arg in extended form is 6–7 Å long, an α-helical span from 49–58 is ~13 Å, and with two extended Arg side chains (~13 Å) yields ~26 Å to span the bilayer (or reach aqueous spaces in contact with the bulk solution). It is important to note that Arg may snorkel to allow exposure to water from MinK sites where the native residue does not; moreover, Arg might travel to water-filled pockets or crevices in the protein rather than gain access to the bulk solution.

Consistent with the idea that a protected stretch begins at residue 50 are studies showing that the pore blocker TEA competes for binding with membrane-impermeant thiol reagents that couple at 44 and 46 (Table 4, Fig. 4 *C*) (14). Also supporting deep intercalation of the TMD into the channel corpus are sites that influence ion selectivity of the pore (16); these coincide with transition from α-helical to alternating periodicity of perturbation (Table 4, Fig. 4 *C*). Other studies have supported contact of TMD residues 58 and 59 and the KCNQ1 pore (19) (Fig. 4 *E*) and observed binding of isolated TMD peptide to the pore (20). Although two other publications argued against contact of the TMD and channel interior based on studies of cadmium inhibition (11,12), the KCNQ1 variant in the first report proved insensitive to pore blockade by cadmium and thus a poor model for wild-type channels (18) and removal of the KCNQ1 cysteine suggested to bind cadmium in the latter report (thereby localizing MinK-55C) to be without impact (18). Subthreshold effects of alterations at 58 (Tables 1–3) despite recognized influence on gating (13,33,37) argue the site does not have strong differential effects on stability of the open compared to the closed state, perhaps because it does not contact parts of the channel that move during gating.

An α-helical model is concordant with sequence analyses and studies of synthetic peptides. Thus, hydrophobicity analysis of the MinK TMD by early (38) and current methods (39) (see Table 4) support the notion that the segment to be α-helical. Indeed, isolated peptide corresponding to the MinK TMD is determined to adopt α-helical conformation when studied by Fourier-transform IR and CD in methanol (40) or proton nuclear magnetic resonance in hexafluoro-isopropanol (41). While peptide incorporation into lipid vesicles by dialysis suggested a predominance of β-sheet in one study (42), this was argued to be aggregation artifact by others who observed primarily α-helix (43).

We favor a model for I_{Ks} channels that has bilateral symmetry for the following reasons (Fig. 4 *E*). A 2:4 ratio of MinK and KCNQ1 subunits in I_{Ks} channels was suggested first based on functional studies (21) and later validated by direct measurement of surface channel number using a radiolabeled pore-binding toxin and accounting of MinK subunits with an antibody-based cell surface luminometry assay (15).

TABLE 4 Effects on I_{Ks} channels of MinK point mutant across the TMD (residues 44–66)

MinK Site	Perturb Trp or Asn	Tolerant Trp + Arg	PROF/PhD analyses	Cd and Zn pore site	Alter ion selectivity	Alter pore blockade	Alter $V_{1/2}$, restore
A44	**High**		L, 9/U, 6			MTSES ↑	
L45	**High**		H, 0/M, 7			TEA 2X↓	
Y46	Low		H, 3/M, 8			MTSES ↑	
V47	**High**		H, 5/M, 8				
L48	Low	Trp + Arg	H, 6/M, 8				
M49	Low	Trp + Arg	H, 7/M, 8				
V50	Low		H, 7/M, 8				
L51	**High**		H, 7/M, 8				
G52	Low		H, 5/M, 8				
F53	Low		H, 7/M, 8			TEA 5X↑	
F54	Low		H, 8/M, 8	External	Cs, NH_4	TEA 5X↑	$V_{1/2}$
G55	**High**		H, 7/M, 8	External	Na	TEA 5X↑, 2X↓	
F56	Low		H, 8/M, 8	Internal			
F57	**High**		H, 7/M, 8				$V_{1/2}$
T58	Low	Trp + Arg	H, 7/M, 8	Internal	Cs, NH_4		$V_{1/2}$, Restore
L59	**High**		H, 8/M, 8				$V_{1/2}$, Restore
G60	Low	Trp + Arg	H, 7/M, 8				
I61	**High**		H, 6/M, 8				$V_{1/2}$
M62	Low	Trp + Arg	H, 7/M, 8				
L63	**High**		H, 6/M, 8				
S64	**High**		H, 4/M, 7				
Y65	Low	Trp + Arg	L, 1/U, 4				
I66	Low	Trp + Arg	L, 8/U, 4				

Perturb Trp or Asn: high and low impact, based on Tables 1 and 2. *Tolerant Trp + Arg*: indicated based on Tables 1 and 3. *PROF/PhD analyses*: support an α-helical TMD from L45 to S64 (39) as reported by earlier methods (38); for *PROF*, *L* indicates ''neither helix nor extended'' and *H* indicates ''helix''; the number is the reliability index of prediction at the site (0 is low and 9 is high); for *PhD*, *U* indicates ''neither helix nor extended'' and *M* indicates ''helix''; the number is the reliability index of prediction at the site (0 is low and 9 is high). *Cd and Zn pore site*: mutations at these sites to Cys create pore sites that mediate blockade by cadmium or zinc added only from the indicated side of the membrane, *External* or *Internal* (16,18). *Alter ion selectivity*: mutations at these sites increase permeation by the indicated ions (13,16). *Alter pore blockade*: mutations at these sites alter pore block by TEA or allow covalent block by MTSES (13,14,17); ↑, higher affinity, ↓, lower affinity; G55 to T 5X ↑; G55 to C 2X ↓; and, MTSES (14). *Alter $V_{1/2}$*, *Restore*: conservative mutations at these sites alter gating or show restoration of function to counteract KCNQ1 mutations and thereby support TMD-KCNQ1 interaction. Based on gating: G54, T58 (13); T58, I61 (33); F57, T58, L59 (20,37); *restore*: entire TMD (20); restorative/interaction sites, T58, L59 (19).

The kinetics of toxin binding to native channels and those with fixed subunit stoichiometry suggested the I_{Ks} outer pore vestibule offers two binding orientations to CTX consistent with bilateral symmetry (15). The perturbation data in this report does not differentiate between a MinK TMD α-helix that travels within one or among multiple KCNQ1 subunits. We prefer the latter hypothesis as MinK and α-subunits appear to assemble during translation (before glycosylation) (44) and evidence that potassium channels form as dimers of α-subunit dimers (45).

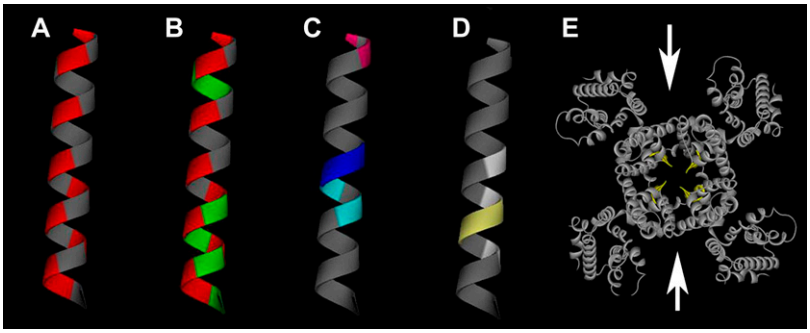

FIGURE 4 MinK TMD sites with impact in I_{Ks} channels presented on an α-helical model. Color-coded based on data in Table 4. (*A*) Red denotes high-impact sites; face with red stripe suggested to contact KCNQ1 protein whereas the opposite face contacts lipid for three turns. (*B*) Green marks sites tolerant of both Trp and Arg and suggests boundaries of access to water; red as in panel *A*. (*C*) Sites mediating pore block and altered ion selectivity; magenta sites are covalently modified by MTSES; dark and light blue mark external and internal cadmium blocking sites, respectively. (*D*) Sites implicated in gating effects; light yellow sites are implicated in direct contact with S6 (19). (*E*) Arrows suggest where MinK might reside in KCNQ1 to yield bilateral symmetry using the membrane portion of Kv1.2 (29) as a model; the bright yellow residues note sites implicated in MinK effects and suggest that portions of MinK intercalate deeply into the pore-forming domains.

Limitations of secondary structure predictions by perturbation with MinK

While perturbation analysis has been used to confirm that spans are peripheral α-helixes, failure to observe periodicity does not prove the converse. Moreover, the findings reported here are equally consistent with a span at the channel-lipid boundary that has a mixed $\alpha-\beta$ structure. While we support a model where the TMD is α-helical and moves from a position of lipid contact to a sequestered milieu based on studies that impugn TMD sites in ion-conduction pore function (Table 4) (13–20), perturbation analysis in this system must be applied with suspicion. Gating energies are, at best, approximated by isochronal measurements required with a channel like I_{Ks} that does not reach steady state. Moreover, contact sites may vary with state, while in this study only the open state has been assessed and, given the absence of saturation, all channels are not in the same conformation when queried. It is also possible that the two MinK subunits in each channel are in nonequivalent locales, although this seems unlikely, based on the pseudo-symmetry observed for identical subunits in potassium channels of known structure and functional support for bilateral symmetry of the I_{Ks} pore (15). Finally, this work was performed without overexpression of other known accessory proteins that modulate I_{Ks} channels such as cAMP-dependent protein kinase, protein phosphatase 1, or their targeting protein Yotiao (46).

Other work

Whereas, the MinK TMD appears to course, in part, through the I_{Ks} channel interior, the accessory subunits of Ca^{2+}-activated potassium channels and K_{ATP} channels are transmembrane proteins thought to interact with their α-subunits solely at the channel periphery (47,48). Similarly, KChiPs and Kvβ type accessory subunits are located in the cytosol peripheral to the ''hanging gondola'' formed by the pore-forming subunits, residing in lateral (49) and inferior locales (29), respectively.

Residues following the MinK TMD are very intolerant to mutation (33,50). For example, the D76N variant that potently depresses I_{Ks} current and was employed to infer subunit stoichiometry by a mixing strategy (21) was later associated with cardiac arrhythmia (7) due to suppression of potassium flux from decreases in both unitary conductance and open probability (9). Perturbation analysis of this nonmembrane embedded MinK region has been performed and revealed effects consistent with α-helical conformation from K69 to A86 bent midway through the course at P77 (51).

We have found that when MinK mutations have significant effects in I_{Ks} channels, the homologous change in MiRP1 or MiRP2 has major impact in the channels they form, even when assembled with disparate pore-forming partners (52). This suggests that if our model for the MinK TMD is valid, it will be recapitulated by other MiRPs.

We thank D. Goldstein for helpful discussions during the course of the study. We are most grateful to J. Rocheleau and W. Kobertz for guidance and hand-holding in the Fourier periodicity analysis and for sharing their data before publication and E. Perozo and V. Jogini for helpful discussions of structural models.

This work was supported by a grant from the National Institutes of Health to S.A.N.G. and the American Heart Association (No. 0635125N) to H.C.

REFERENCES

1. Abbott, G. W., and S. A. N. Goldstein. 1998. A superfamily of small potassium channel subunits: form and function of the MinK-related peptides (MiRPs). *Q. Rev. Biophys.* 31:357–398.
2. Abbott, G. W., F. Sesti, I. Splawski, M. Buck, M. H. Lehmann, K. W. Timothy, M. T. Keating, and S. A. N. Goldstein. 1999. MiRP1 forms IKr potassium channels with HERG and is associated with cardiac arrhythmia. *Cell.* 97:175–187.
3. Cai, S.-Q., L. Hernandez, Y. Wang, K. H. Park, and F. Sesti. 2005. MPS-1 is a K^+ channel β-subunit and a serine-threonine kinase. *Nat. Neurosci.* 8:1503–1509.
4. McCrossan, Z. A., and G. W. Abbott. 2004. The MinK-related peptides. *Neuropharma.* 47:787–821.
5. Sanguinetti, M. C., M. E. Curran, A. Zou, J. Shen, P. S. Spector, D. L. Atkinson, and M. T. Keating. 1996. Coassembly of KvLQT1 and Mink (Isk) proteins to form cardiac I_{Ks} potassium channel. *Nature.* 384:80–83.
6. Barhanin, J., F. Lesage, E. Guillemare, M. Fink, M. Lazdunski, and G. Romey. 1996. KvLQT1 and IsK (minK) proteins associate to form the I_{Ks} cardiac potassium current. *Nature.* 384:78–80.
7. Splawski, I., K. W. Timothy, G. M. Vincent, A. D. L. Atkinson, and M. T. Keating. 1997. Molecular basis of the long-QT syndrome associated with deafness. *N. J. Med.* 336:1562–1567.
8. Schulze-Bahr, E., Q. Wang, H. Wedekind, W. Haverkamp, Q. Chen, and Y. Sun. 1997. KCNE1 mutations cause Jervell and Lange-Nielsen syndrome. *Nat. Genet.* 17:267–268.
9. Sesti, F., and S. A. N. Goldstein. 1998. Single-channel characteristics of wild-type I_{Ks} channels and channels formed with two minK mutants that cause long QT syndrome. *J. Gen. Physiol.* 112:651–664.
10. Splawski, I., J. Shen, K. W. Timothy, M. H. Lehmann, S. Priori, J. L. Robinson, A. J. Moss, P. J. Schwartz, J. A. Towbin, G. M. Vincent, and M. T. Keating. 2000. Spectrum of mutations in long-QT syndrome genes. KVLQT1, HERG, SCN5A, KCNE1, and KCNE2. *Circulation.* 102:1178–1185.
11. Kurokawa, J., H. K. Motoike, and R. S. Kass. 2001. TEA^+-sensitive KCNQ1 constructs reveal pore-independent access to KCNE1 in assembled I_{Ks} channels. *J. Gen. Physiol.* 117:43–52.
12. Tapper, A. R., and A. L. J. George. 2001. Location and orientation of minK within the IKs potassium channel complex. *J. Biol. Chem.* 276: 38249–38254.
13. Goldstein, S. A., and C. Miller. 1991. Site-specific mutations in a minimal voltage-dependent K^+ channel alter ion selectivity and open-channel block. *Neuron.* 7:403–408.
14. Wang, K.-W., K.-K. Tai, and S. A. N. Goldstein. 1996. MinK residues line a potassium channel pore. *Neuron.* 16:571–577.
15. Chen, H., L. A. Kim, S. Rajan, S. Xu, and S. A. N. Goldstein. 2003. Charybdotoxin binding in the I_{Ks} pore demonstrates two MinK subunits in each channel complex. *Neuron.* 40:15–23.
16. Tai, K. K., and S. A. N. Goldstein. 1998. The conduction pore of a cardiac potassium channel. *Nature.* 391:605–608.
17. Sesti, F., K. K. Tai, and S. A. N. Goldstein. 2000. MinK endows the I_{Ks} potassium channel with sensitivity to internal TEA. *Biophys. J.* 79:1369–1378.
18. Chen, H., F. Sesti, and S. A. N. Goldstein. 2003. Pore and state-dependent cadmium block of I_{Ks} channels formed with MinK-55C and wild-type KCNQ1 subunits. *Biophys. J.* 84:3679–3689.

19. Panaghie, G., K.-K. Tai, and G. W. Abbott. 2006. Interaction of KCNE subunits with the KCNQ1 K^+ channel pore. *J. Physiol.* 570:455–467.

20. Melman, Y. F., S. Y. Um, A. Krumerman, A. Kagan, and T. V. McDonald. 2004. KCNE1 binds to the KCNQ1 pore to regulate potassium channel activity. *Neuron.* 42:927–937.

21. Wang, K. W., and S. A. N. Goldstein. 1995. Subunit composition of minK potassium channels. *Neuron.* 14:1303–1309.

22. Choe, S., C. F. Stevens, and J. M. Sullivan. 1995. Three distinct structural environments of a transmembrane domain in the inwardly rectifying potassium channel ROMK1 defined by perturbation. *Proc. Natl. Acad. Sci. USA.* 92:12046–12049.

23. Collins, A., H.-h. Chuang, Y. N. Jan, and L. Y. Jan. 1997. Scanning mutagenesis of the putative transmembrane segments of Kir2.1, an inward rectifier potassium channel. *Proc. Natl. Acad. Sci. USA.* 94:5456–5460.

24. Jones, J. D., and L. M. Gierasch. 1994. Effect of charged residue substitutions on the membrane-interactive properties of signal sequences of the *Escherichia coli* LamB protein. *Biophys. J.* 67:1534–1545.

25. Segrest, J. P., H. De Loof, J. G. Dohlman, C. G. Brouilette, and G. M. Anantharamaiah. 1990. Amphipathic helix motif: classes and properties. *Proteins Struct. Funct. Genet.* 8:103–117.

26. Monks, S. A., D. J. Needleman, and C. Miller. 1999. Helical structure and packing orientation of the S2 segment in the *Shaker* K^+ channel. *J. Gen. Physiol.* 113:415–423.

27. Hong, K. H., and C. Miller. 2000. The lipid-protein interface of a *Shaker* K^+ channel. *J. Gen. Physiol.* 115:51–58.

28. Li-Smerin, Y., D. H. Hackos, and K. J. Swartz. 2000. α-Helical structural elements within the voltage-sensing domains of a K^+ channel. *J. Gen. Physiol.* 115:33–50.

29. Long, S. B., E. B. Campbell, and R. MacKinnon. 2005. Crystal structure of a mammalian voltage-dependent *Shaker* family K^+ channel. *Science.* 309:897–903.

30. Bockenhauer, D., N. Zilberberg, and S. A. N. Goldstein. 2001. KCNK2: reversible conversion of a hippocampal potassium leak into a voltage-dependent channel. *Nat. Neurosci.* 4:486–491.

31. Hausdorff, S. F., S. A. Goldstein, E. E. Rushin, and C. Miller. 1991. Functional characterization of a minimal K^+ channel expressed from a synthetic gene. *Biochemistry.* 30:3341–3346.

32. Goldstein, S. A., and C. Miller. 1993. Mechanism of charybdotoxin block of a voltage-gated K^+ channel. *Biophys. J.* 65:1613–1619.

33. Takumi, T., K. Moriyoshi, I. Aramori, T. Ishii, S. Oiki, Y. Okada, H. Ohkubo, and S. Nakanishi. 1991. Alteration of channel activities and gating by mutations of slow ISK potassium channel. *J. Biol. Chem.* 266:22192–22198.

34. Busch, A. E., M. D. Varnum, R. A. North, and J. P. Adelman. 1992. An amino acid mutation in a potassium channel that prevents inhibition by protein kinase C. *Science.* 255:1705–1707.

35. Sesti, F., G. W. Abbott, J. Wei, K. T. Murray, S. Saksena, P. J. Schwartz, S. G. Priori, D. M. Roden, A. L. George, Jr., and S. A. Goldstein. 2000. A common polymorphism associated with antibiotic-induced cardiac arrhythmia. *Proc. Natl. Acad. Sci. USA.* 97:10613–10618.

36. Hildebrand, P. W., R. Preissner, and C. Frömmel. 2004. Structural features of transmembrane helices. *FEBS Lett.* 559:145.

37. Melman, Y. F., A. Domenech, S. de la Luna, and T. V. McDonald. 2001. Structural determinants of KvLQT1 control by the KCNE family of proteins. *J. Biol. Chem.* 276:6439–6444.

38. Takumi, T., H. Ohkubo, and S. Nakanishi. 1988. Cloning of a membrane protein that induces a slow voltage-gated potassium current. *Science.* 242:1042–1045.

39. Rost, B., R. Casadio, and P. Fariselli. 1996. Topology prediction for helical transmembrane proteins at 86% accuracy. *Protein Sci.* 5:1704–1718.

40. Ben-Efraim, I., D. Bach, and Y. Shai. 1993. Spectroscopic and functional characterization of the putative transmembrane segment of the minK potassium channel. *Biochemistry.* 9:2371–2377.

41. Aggeli, A., M. L. Bannister, M. Bell, N. Boden, J. B. C. Findlay, M. Hunter, P. F. Knowles, and J.-C. Yang. 1998. conformation and ion-channeling activity of a 27-residue peptide modeled on the single-transmembrane segment of the IsK (minK) protein. *Biochemistry.* 37: 8121–8131.

42. Horváth, L. I., T. Heimburg, P. Kovachev, J. B. Findlay, K. Hideg, and D. Marsh. 1995. Integration of a K^+ channel-associated peptide in a lipid bilayer: conformation, lipid-protein interactions, and rotational diffusion. *Biochemistry.* 38:3893–3898.

43. Mercer, E. A., G. W. Abbott, S. P. Brazier, B. Ramesh, P. I. Haris, and S. K. Srai. 1997. Synthetic putative transmembrane region of minimal potassium channel protein (minK) adopts an α-helical conformation in phospholipid membranes. *Biochem. J.* 325:475–479.

44. McDonald, T. V., Z. Yu, Z. Ming, E. Palma, M. B. Meyers, K. W. Wang, S. A. N. Goldstein, and G. I. Fishman. 1997. A minK-HERG complex regulates the cardiac potassium current IKr. *Nature.* 388:289–292.

45. Tu, L., and C. Deutsch. 1999. Evidence for dimerization of dimers in K^+ channel assembly. *Biophys. J.* 76:2004–2017.

46. Marx, S. O., J. Kurokawa, S. Reiken, H. Motoike, J. D'Armiento, A. R. Marks, and R. S. Kass. 2002. Requirement of a macromolecular signaling complex for β-adrenergic receptor modulation of the KCNQ1-KCNE1 potassium channel. *Science.* 295:496–499.

47. Wallner, M., P. Meera, and L. Toro. 1996. Determinant for β-subunit regulation in high-conductance voltage-activated and Ca^{2+}-sensitive K^+ channels: an additional transmembrane region at the N terminus. *Proc. Natl. Acad. Sci. USA.* 93:14922–14927.

48. Clement, J. P. T., K. Kunjilwar, G. Gonzalez, M. Schwanstecher, U. Panten, L. Aguilar-Bryan, and J. Bryan. 1997. Association and stoichiometry of K_{ATP} channel subunits. *Neuron.* 185:827–838.

49. Kim, L. A., J. Furst, D. Gutierrez, M. H. Butler, S. Xu, S. A. Goldstein, and N. Grigorieff. 2004. Three-dimensional structure of I(to); Kv4.2-KChIP2 ion channels by electron microscopy at 21 Ångstrom resolution. *Neuron.* 41:513–519.

50. Gage, S. D., and W. R. Kobertz. 2004. KCNE3 truncation mutants reveal a bipartite modulation of KCNQ1 K^+ channels. *J. Gen. Physiol.* 124:759–771.

51. Rocheleau, J. M., S. D. Gage, and W. R. Kobertz. 2006. Secondary structure of a KCNE cytoplasmic domain. *J. Gen. Physiol.* 128: 721–729.

52. Abbott, G. W., and S. A. Goldstein. 2002. Disease-associated mutations in KCNE potassium channel subunits (MiRPs) reveal promiscuous disruption of multiple currents and conservation of mechanism. *FASEB J.* 16:390–400.